Available online at www.sciencedirect.com
SCIENCE DIRECT
Tectonophysics 418 (2006) 145–162
TECTONOPHYSICS
www.elsevier.com/locate/tecto

Magnetic fabric variations in Mesozoic black shales, Northern Siberia, Russia: Possible paleomagnetic implications

Martin Chadima [a,*], Petr Pruner [a], Stanislav Šlechta [a], Tomáš Grygar [b], Ann M. Hirt [c]

[a] Institute of Geology, Academy of Sciences, Rozvojová 135, CZ-16502 Prague, Czech Republic
[b] Institute of Inorganic Chemistry, Academy of Sciences, CZ-25068 Rež, Czech Republic
[c] Institut für Geophysik, ETH-Hönggerberg, CH-8093 Zürich, Switzerland

Received 13 June 2005; received in revised form 20 October 2005; accepted 5 December 2005
Available online 28 February 2006

Abstract

A 28-m-long section situated on the coast of the Arctic Ocean, Russia (74°N, 113°E) was extensively sampled primarily for the purpose of magnetostratigraphic investigations across the Jurassic/Cretaceous boundary. The section consists predominantly of marine black shales with abundant siderite concretions and several distinct siderite cemented layers. Low-field magnetic susceptibility (k) ranges from 8×10^{-5} to 2×10^{-3} SI and is predominantly controlled by the paramagnetic minerals, i.e. iron-bearing chlorites, micas, and siderite. The siderite-bearing samples possess the highest magnetic susceptibility, usually one order of magnitude higher than the neighboring rock. The intensity of the natural remanent magnetization (M_0) varies between 1×10^{-5} and 6×10^{-3} A/m. Several samples possessing extremely high values of M_0 were found. There is no apparent correlation between the high k and high M_0 values; on the contrary, the samples with relatively high M_0 values possess average magnetic susceptibility and vice versa. According to the low-field anisotropy of magnetic susceptibility (AMS), three different groups of samples can be distinguished. In the siderite-bearing samples (i), an inverse magnetic fabric is observed, i.e., the maximum and minimum principal susceptibility directions are interchanged and the magnetic fabric has a distinctly prolate shape. Triaxial-fabric samples (ii), showing an intermediate magnetic fabric, are always characterized by high M_0 values. It seems probable that the magnetic fabric is controlled by the preferred orientation of paramagnetic phyllosilicates, e.g., chlorite and mica, and by some ferromagnetic mineral with anomalous orientation in relation to the bedding plane. Oblate-fabric samples (iii) are characterized by a bedding-controlled magnetic fabric, and by moderate magnetic susceptibility and M_0 values. The magnetic fabric is controlled by the preferred orientation of phyllosilicate minerals and, to a minor extent, by a ferrimagnetic fraction, most probably detrital magnetite. Considering the magnetic fabric together with paleomagnetic component analyses, the siderite-bearing, and the high-NRM samples (about 15% of samples) were excluded from further magnetostratigraphic research.

Keywords: AMS; AARM; High-field anisotropy; Inverse magnetic fabric; Siderite; Jurassic/Cretaceous boundary

1. Introduction

Recent magnetostratigraphic investigations across the Jurassic/Cretaceous (J/K) boundary carried out on three representative sections in the Tethyan realm of Europe yielded comparable results (Houša et al., 1999, 2004). In order to establish a magnetostratigraphic correlation with the Boreal realm, a section across the J/K boundary was studied in the Eastern Russian Arctic. As a complementary technique to magnetostratigraphy, the measurements of the anisotropy of the

* Corresponding author. Tel.: +42 272 690 115.
E-mail address: chadima@sci.muni.cz (M. Chadima).

0040-1951/$ - see front matter © 2006 Elsevier B.V. All rights reserved.
doi:10.1016/j.tecto.2005.12.018

low-field magnetic susceptibility (AMS) were performed throughout the section. Unexpectedly, several different orientations and shapes of magnetic fabric ellipsoid were found. The AMS of any rock is dependent on the intrinsic magnetic susceptibility, volume fraction, and degree of preferred orientation of the individual rock-constituent minerals. For this reason the AMS reflects not only the differences in the rock fabric but also any mineralogical variations within the studied rock units (e.g. Robion et al., 1995). Such variations, if caused by the presence of different types of ferromagnetic minerals (e.g. Lehman et al., 1996), may lead to erroneous magnetostratigraphic interpretations and should be, therefore, thoroughly understood.

In sedimentary rocks unaffected by tectonic ductile deformation, the so-called 'normal magnetic fabric' is usually observed. The normal magnetic fabric is characterized by magnetic foliation oriented parallel to the bedding, and magnetic lineation being roughly parallel to the near-bottom water current direction or, in special cases, perpendicular to it (Hamilton and Rees, 1970). The magnitude of the sedimentary magnetic fabric is relatively low and the fabric is distinctly oblate. Despite the predominant occurrence of normal magnetic fabrics, 'inverse magnetic fabrics' are observed in the sedimentary rocks containing minerals with an inverse relationship between magnetic axes and shape and/or crystallographic axes (e.g. Rochette, 1988). In rocks possessing the inverse fabric, the principal magnetic axes are inverted, thus, both magnetic foliation and magnetic lineation are perpendicular to the bedding plane and the fabric is distinctly prolate (Rochette et al., 1992). Inverse magnetic fabric can be carried by single-domain magnetite (Potter and Stephenson, 1988; Rochette et al., 1999; Borradaile and Gauthier, 2001), tourmaline (Rochette et al., 1994; Ferré and Améglio, 2000), cordierite, goethite (Lehman et al., 1996), or by different iron-bearing carbonates (Ellwood et al., 1986; Rochette, 1988; Ellwood et al., 1989; Ihmlé et al., 1989; Winkler et al., 1996; Hounslow, 2001; de Wall and Warr, 2004).

The purpose of the present paper is to interpret the different types of magnetic fabric found in the studied sedimentary rocks. An integrated magnetic fabric approach (AMS, high-field anisotropy, anisotropy of anhysteretic remanent magnetization) is combined with standard magnetic and non-magnetic mineral identification techniques. The understanding of the mineralogical control on magnetic fabric is used to help discriminate which samples are unsuitable for a reliable magnetostratigraphy.

2. Geological setting and sampling

The magnetostratigraphic and magnetic fabric investigation was carried out in a sedimentary complex exposed on the coast of the Laptev Sea (Zakharov et al., 1983). The sedimentary sequence was deposited in a foreland basin on the passive continental margin bounding the Siberian Craton to the north. The rocks from the foreland basin were subsequently deformed by folding and thrusting in the Early Cretaceous (Drachev et al., 1998).

The studied outcrop is located on the Nordvik Peninsula, Urdyuk-Khaya Cape, west coast of the Anabar Bay (73°54′N, 113°04′E, Fig. 1a). The rocks representing the supposed J/K boundary interval are exposed as a broad syncline with the dip of strata changing progressively from subhorizontal to approximately 60°. Several faults with adjacent zones of brittle deformation cross-cut the outcrop. The section is composed of marine mudstones and siltstones, which we will denote as shales, with abundant concretions and several distinct cemented layers (Fig. 1b). A newly formed siderite was observed macroscopically in the concretions and cemented layers. In addition to siderite, several horizons with small pyrite nodules and thin pyrite layers were present within the shales (Fig. 1b). The main constituents of the studied shales, which have been identified by microscopic observations, are rock fragments, quartz, feldspars, micas, chlorites, glauconite and pyrite (Zakharov et al., 1983).

Overall 370 oriented samples were taken from three individual sections (Fig. 1b). The H- and D-sections were sampled above and below the supposed J/K boundary, respectively. This boundary is marked by a 4- to 6-cm-thick phosphate limestone horizon with high contents of iridium and other noble metals (Zakharov et al., 1993). Due to the occurrence of the fault zones, a continuation of the D-section was sampled several hundred meters away, denoted as M-section. Approximately 2-m overlap interval between the D- and M-section was sampled in order to ensure the correct linking (Fig. 1b). Sample names include the acronym of the respective section plus figure expressing the distance of the sample from the supposed J/K boundary in cm. In the central part, dense sampling at 2–4 cm spacing was made (D-section), whereas the marginal parts were sampled at approximately 10-cm intervals (H- and M-sections). The samples were cut as 2×2×2 cm cubes directly from the outcrop, using a diamond-coated wheel saw. In order to prevent further disintegration of the very loose sediment, each sample was pressed into a plastic

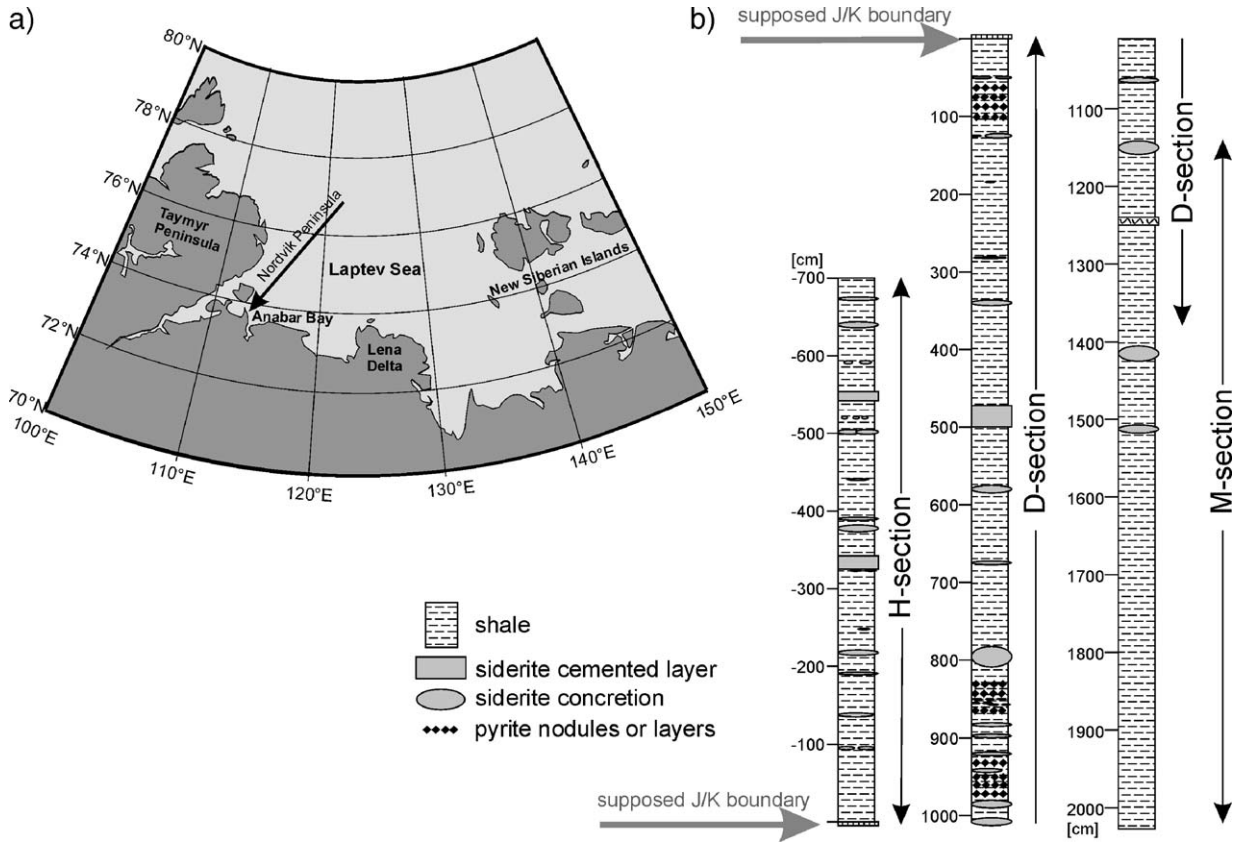

Fig. 1. Location (a) and the lithological log (b) of the studied section on the Nordvik Peninsula, Northern Siberia, Russia. The log is labeled in cm, with negative or positive numbers denoting positions above or below the supposed Jurassic/Cretaceous boundary, respectively. Lithological log drawn by M. Mazuch.

cube. A significant limitation to using plastic cases is that samples cannot be thermally demagnetized or subjected to any thermal rock magnetic analysis.

3. Laboratory techniques and data processing

3.1. Identification of magnetic minerals

Temperature variations of magnetic susceptibility from room temperature up to 700 °C were measured with an Agico KLY-4S Kappabridge coupled with a temperature control apparatus CS-3. All the measurements were performed on powdered samples in air atmosphere, with a heating rate of approximately 10 °C/min. The curves of the temperature dependence of magnetic susceptibility allow the resolution of the room temperature susceptibility into its paramagnetic and ferromagnetic components based on the hyperbola-fitting method (Hrouda, 1994; Hrouda et al., 1997).

In order to test for the presence of pyrrhotite, bulk susceptibility was measured as a function of applied AC field with an Agico KLY-4S Kappabridge. The field intensity was gradually increased from 2 to 450 A/m.

An isothermal remanent magnetization (IRM) was acquired progressively using a Magnetic Measurements MMPM10 pulse magnetizer in fields up to 1 T. The acquired IRM was measured after each imparted field with an Agico JR-5 spinner magnetometer. Backfield demagnetization was done using a pulse magnetizer. The *S*-ratio was calculated according to Bloemendal et al. (1992):

$$S_{-0.3\ \mathrm{T}} = [-(\mathrm{IRM}_{-0.3\mathrm{T}}/\mathrm{SIRM}) + 1]/2$$

where SIRM is the saturation IRM, which was imparted applying an IRM in one direction in a maximum field of 1 T, and $\mathrm{IRM}_{-0.3\mathrm{T}}$ is the magnetization after the application of 300 mT field in the opposite direction. All the rock magnetic measurements were carried out in the Paleomagnetic laboratory, Institute of Geology, Prague, Czech Republic.

The X-ray diffraction (XRD) was done using a Siemens D5005 diffractometer in the Institute of

Inorganic Chemistry, Řež, Czech Republic. The diffractometer is equipped with a Cu X-ray source with a wavelength $\lambda = 1.54$ Å. The diffraction scans were made on powder samples in the range of 2θ angle from 2° to 80° with angular velocity of 1°/min.

Backscattered electron (BSE) images on polished sections were done using a Cameca SX-100 Electron Probe MicroAnalyzer having four wave-dispersive spectrometers (WDS) in the Institute of Geology, Prague.

3.2. Natural remanent magnetization

The natural remanent magnetization (NRM) was investigated to study the magnetic polarity for magnetostratigraphic purposes in the Geological Research Center, Potsdam, Germany. Stepwise alternating field (AF) demagnetization up to a maximum field of 100 mT was performed with a 2G Enterprises degausser system. After each demagnetization step, the remanent magnetization was measured on a 2G Enterprises cryogenic magnetometer. Characteristic remanent magnetization (ChRM) directions were identified from vector-component diagrams using principal component analysis (Kirschvink, 1980). The mean ChRM directions were analyzed using the statistics on sphere (Fisher, 1953).

3.3. Magnetic fabric

The AMS and the anisotropy of anhysteretic remanent magnetization (AARM) was studied in the Paleomagnetic laboratory in Prague. The AMS was measured with an Agico KLY-4S Kappabridge with an alternating field intensity of 300 A/m and operating frequency of 875 Hz. The AARM was measured using an Agico AF demagnetizer/magnetizer LDA-3/AMU-1 and an Agico JR-6 spinner magnetometer. The remanent magnetization was imparted in six pairs of antiparallel directions with a DC field of 100 μT and AC field of 50 mT. Using this measurement design, the 'hard' magnetization components, which cannot be demagnetized, are reasonably eliminated (Jelínek, 1993). A tumbling system was used to demagnetize the samples after each pair of magnetizing positions.

The high-field magnetic anisotropy (HFA) was measured using a high-field torque magnetometer (Bergmüller et al., 1994) in the Laboratory for Natural Magnetism, Institute of Geophysics, ETH, Zürich, Switzerland. In the high-field torque magnetometer, a sample is measured along three mutually perpendicular axes with an angular increment of 20° in four different fields. These fields were strong enough to saturate ferrimagnetic minerals and allowed the separation of paramagnetic and ferrimagnetic contribution to the magnetic anisotropy using the method of Martín-Hernández and Hirt (2001).

The magnetic anisotropy (either AMS, AARM, or HFA) can be mathematically described as a symmetric second rank tensor which can be visualized as an ellipsoid. Its semi-axes lengths, $k_1 \geq k_2 \geq k_3$, are termed principal values and their orientations, $\mathbf{K}_1$, $\mathbf{K}_2$, $\mathbf{K}_3$, are denoted as principal directions. In the framework of magnetic fabric, the maximum direction ($\mathbf{K}_1$) defines a magnetic lineation while the plane perpendicular to minimum direction ($\mathbf{K}_3$) and containing maximum and intermediate directions ($\mathbf{K}_1$, $\mathbf{K}_2$) defines a magnetic foliation.

Quantitatively, the magnetic anisotropy is presented in terms of the mean susceptibility, k (applies to the AMS), the degree of anisotropy P (AMS, AARM), the shape parameter, T (AMS, AARM), and the difference shape factor, U (AMS, HFA) defined as follows:

$$k = (k_1 + k_2 + k_3)/3 \quad \text{(Nagata, 1961)}$$

$$P = k_1/k_3 \quad \text{(Nagata, 1961)}$$

$$T = 2\ln(k_2/k_3)/\ln(k_1/k_3) - 1 \quad \text{(Jelínek, 1981)}$$

$$U = (2k_2 - k_1 - k_3)/(k_1 - k_3) = [2(k_2 - k) - (k_1 - k) - (k_3 - k)]/[(k_1 - k) - (k_3 - k)] \quad \text{(Jelínek, 1981)}$$

where $(k_1 - k) \geq (k_2 - k) \geq (k_3 - k)$ are the deviatoric principal values.

The P parameter indicates the magnitude of the magnetic anisotropy and the T parameter indicates the shape of the anisotropy ellipsoids; it varies from −1 (perfectly prolate magnetic fabric) to +1 (perfectly oblate magnetic fabric). The employment of the infrequently used difference shape factor, U, arises from the intended comparison of the AMS with the HFA. As the torque magnetometer measures only the deviatoric component of anisotropy, only the U parameter based on the susceptibility differences can be calculated. The shape difference factor, U, is analogous to the T shape factor, ranging from −1 to 1; negative or positive values indicate prolate- or oblate-fabrics, respectively.

4. Magnetic mineralogy

A number of samples have been subjected to magnetic and non-magnetic mineral identification techniques, and three types of magnetic behavior can be identified. For this reason, data from three representative samples are presented. The basic parameters of NRM and AMS for these samples are summarized in Table 1.

Table 1
The basic parameters of NRM and AMS for representative samples

Sample	M_0	MDF	k	P	T	Inc $\mathbf{K}_1$	Inc $\mathbf{K}_2$	Inc $\mathbf{K}_3$
D0653	5.01×10^{-2}	25.6	201.6×10^{-6}	1.092	0.022	8.4	68.7	19.4
D0907	3.31×10^{-4}	18.7	206.0×10^{-6}	1.055	0.995	13.3	6.4	75.2
D1245	1.74×10^{-4}	26.5	1055.3×10^{-6}	1.150	−0.990	81.7	1.9	8.1

M_0, intensity of natural remanent magnetization in A/m; MDF, medium destructive field in mT; k, mean susceptibility in 10^{-6} SI; P, magnitude of AMS; T, shape parameter of AMS; Inc $\mathbf{K}_1$, Inc $\mathbf{K}_2$, Inc $\mathbf{K}_3$, inclinations of maximum, intermediate, and minimum susceptibility directions, respectively, in bedding coordinate system (tilt correction).

4.1. Temperature variation of magnetic susceptibility

During the laboratory heating of the powder samples, the magnetic susceptibility decreases as a function of increasing temperature following a paramagnetic hyperbola according to the Curie–Weiss law (Fig. 2). Depending on the sample, the hyperbolic decrease is maintained up to the temperature of 240 or 300 °C. Susceptibility resolution in the low-temperature hyperbolic interval showed that room temperature bulk magnetic susceptibility is dominated by the paramagnetic fraction. Paramagnetic contribution to the room temperature bulk susceptibility ranges from approximately 80% to 100% (Fig. 2).

Two different sample behaviors are observed above the temperature of 240 or 300 °C. For some samples, the susceptibility starts to increase after 240 °C, first slowly, and above 290 °C, rapidly. The slope of the curve changes again in the temperature interval between 340 and 390 °C where a gentle increase is evident (Fig. 2, D0653). Above 390 °C, the magnetic susceptibility reaches values an order of magnitude higher than original room temperature magnetic susceptibility. Above 500 °C, the magnetic susceptibility starts to decrease rapidly, and later above 580 °C, follows a hyperbolic curve.

For the second group of samples, the shoulder in the susceptibility increase in the 240–390 °C interval is not present. Magnetic susceptibility starts to increase rapidly at temperatures above 300 °C (Fig. 2, D0907, D1245) reaching maximum values of one or two orders of magnitude higher than the original room temperature magnetic susceptibility. The susceptibility starts to decrease above the temperature of 520–545 °C, and follows again a hyperbolic course in the interval above approximately 580 °C (D0907) or 625 °C (D1245).

4.2. X-ray diffraction and electron microscopy

The diffraction scans vary according to the studied sample. The pronounced peaks corresponding to the X-ray diffractions on various structural planes of quartz, feldspars (albite and microcline), muscovite, chlorite (clinochlore), siderite, pyrite, gypsum, and kaolinite were identified (Fig. 3). The semi-quantitative phase composition estimates based on the relative intensity

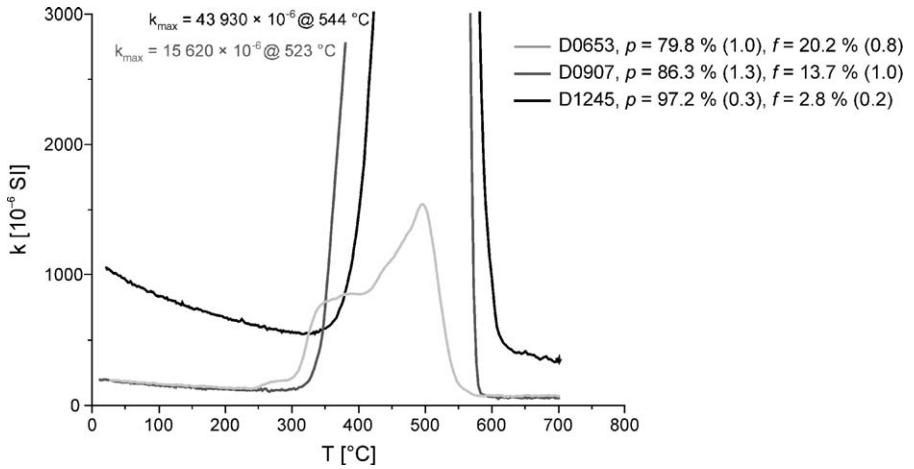

Fig. 2. Temperature variations of bulk magnetic susceptibility. Test samples were heated in the air atmosphere with a heating rate of 10 °C/min. The resolution of the room susceptibility into the paramagnetic (p) and ferromagnetic (f) component with the standard deviations (in parenthesis) is presented for each curve.

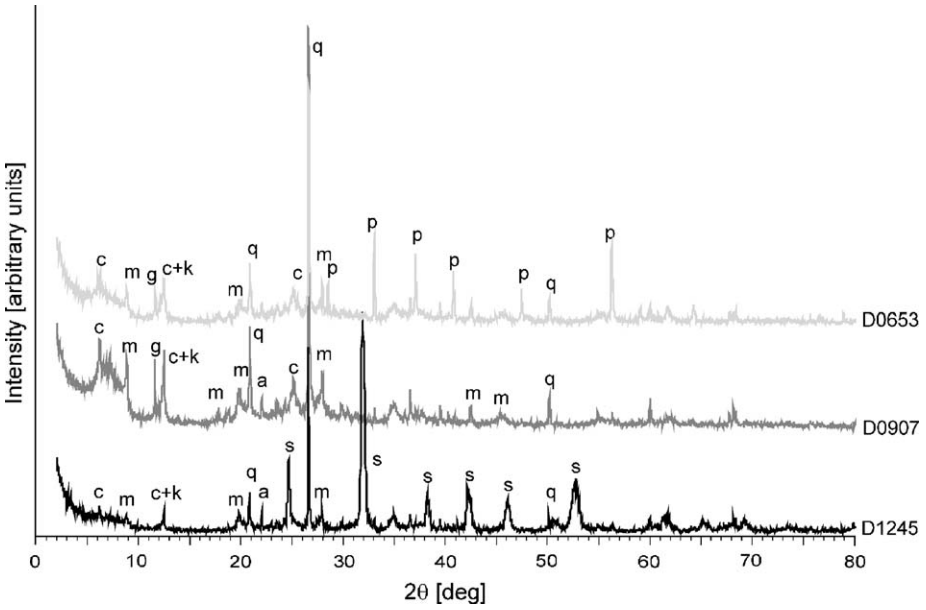

Fig. 3. The X-ray powder diffraction scans for three test samples in the range of 2θ angle 2°–80° with angular velocity 1°/min. The main diffraction peaks of the rock-constituent minerals are labeled: quartz (q), muskovite (m), clinochlore (c), siderite (s), pyrite (p), gypsum (g), albite (a), and kaolinite (k).

ratios referring to corundum standard are presented in Table 2. In the BSE images the zonal nodules, corroded euhedral crystals and framboides are observed in phyllosilicate matrix (Fig. 4). The atomic weight ratios derived from WDS analyses of nodules, crystals and framboides are close to the composition of pyrite.

4.3. Ferromagnetic mineralogy

Several methods of rock magnetic analysis were used to identify the ferromagnetic mineralogy of the rocks. The acquisition of IRM showed that all samples reached magnetic saturation by 200 to 500 mT (Fig. 5a). Backfield demagnetization of the saturation IRM (SIRM) revealed a coercivity of remanence, H_{cr}, between 30 to 50 mT in general. One sample had a H_{cr} around 53 mT (Fig. 5a, D1245).

In order to test for the presence of pyrrhotite, bulk susceptibility was measured as a function of applied AC field (Worm et al., 1993, Pokorný et al., 2004). No field dependence is observed in the test samples and bulk magnetic susceptibility remains constant during gradual increase of the AC field from 2 to 450 A/m (Fig. 5b).

5. Magnetic fabric and NRM

5.1. Theoretical models of inverse and anomalous magnetic fabric

The origin of the inverse, and intermediate magnetic fabrics was reviewed and modeled by Rochette et al. (1992, 1999), and Ferré (2002). In these models, the terms normal, inverse, intermediate, and anomalous magnetic fabric were defined according to the relationship of the principal anisotropy directions to the principal directions of structural features. 'Normal' is used to describe a magnetic fabric whose $\mathbf{K}_1$ direction is parallel to a structural lineation (either flow, current, stretching direction, or apparent lineation), and whose $\mathbf{K}_3$ direction is normal to a structural foliation (e.g., plane of flattening, flow or bedding plane, Fig. 6, N). Strictly following the directional definition, the normal

Table 2
The semi-quantitative phase composition estimates (%) of the rock-constituent minerals on the basis of the relative intensity XRD ratios referring to corundum standard

Sample	Quartz	Pyrite	Albite	Muscovite	Clinoclore	Siderite	Gypsum	Kaolinite	Microcline
D0653	27.6	18.2	3.0	37.1	8.1		5.9		
D0907	25.5	2.0	2.4	44.5	8.8		9.4	5.6	1.9
D1245	43.4	4.9	7.2	21.0	7.5	16.1			

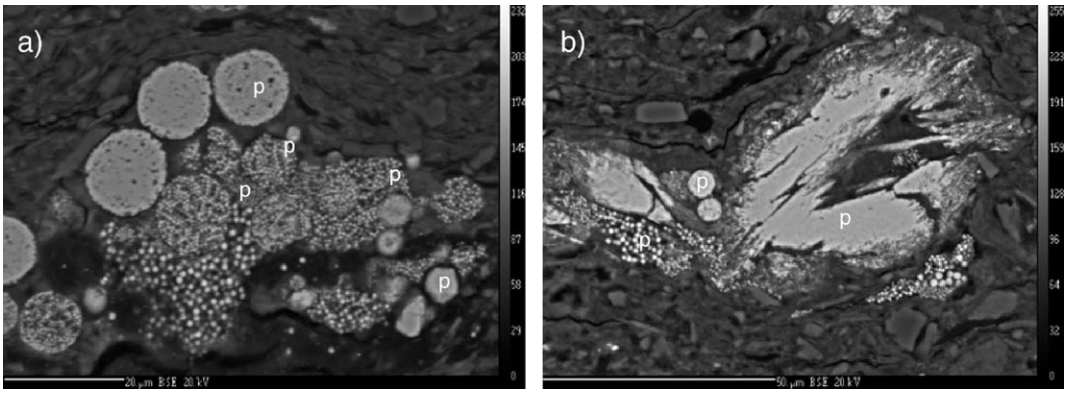

Fig. 4. Backscattered electron images of the polished sections of the representative pyrite-bearing sample with different types of pyrite (p) in phyllosilicate matrix. (a) Pyrite nodules, corroded euhedral crystals and framboides, (b) large corroded pyrite crystal.

magnetic fabric can be in principle oblate, triaxial, or prolate in symmetry. In the 'inverse' magnetic fabric, the maximum and minimum anisotropy axes are inverted relative to the normal fabric (Fig. 6, I). The origin of intermediate fabric has been modeled by mixing the normal and inverse fabric end-members (Rochette et al., 1992; Ferré, 2002). Depending on the anisotropy degree and the symmetry of the end-members, different types of intermediate fabrics can theoretically develop. No intermediate fabric develops when a normal and inverse end-member with the inverted symmetry are mixed. When the oblate-normal and prolate-inverse end-members are mixed the 'false normal' ($\mathbf{K}_1$ and $\mathbf{K}_2$ are interchanged, Fig. 6, FN), and later, the 'intermediate' (further interchange of $\mathbf{K}_2$ and $\mathbf{K}_3$, Fig. 6, IM1) fabrics develop. When the prolate-normal and prolate-inverse end-members are mixed the 'intermediate' ($\mathbf{K}_2 \leftrightarrow \mathbf{K}_3$, Fig. 6, IM2) and the 'false inverse' (further exchange of $\mathbf{K}_1$ and $\mathbf{K}_2$, Fig. 6, FI) fabrics develop. Anomalous fabric is characterized by a random distribution of magnetic axes (Fig. 6, A).

When no structural lineation is observed in the field, the orientation of magnetic fabric can be solely related to the structural foliation, e.g. bedding plane in undeformed sedimentary rocks, using the inclination of principal anisotropy directions. In such a simplified scheme, the 'false normal', and 'false inverse' fabrics (cf. Rochette et al., 1999) cannot be distinguished. In order to fully evaluate all possible orientations of magnetic fabrics, the ternary diagram interrelating inclinations of all three principal anisotropy directions in bedding coordinates is introduced (Fig. 6). In such a ternary diagram, the normal, and inverse magnetic fabrics plot in the close vicinity of the lower left and

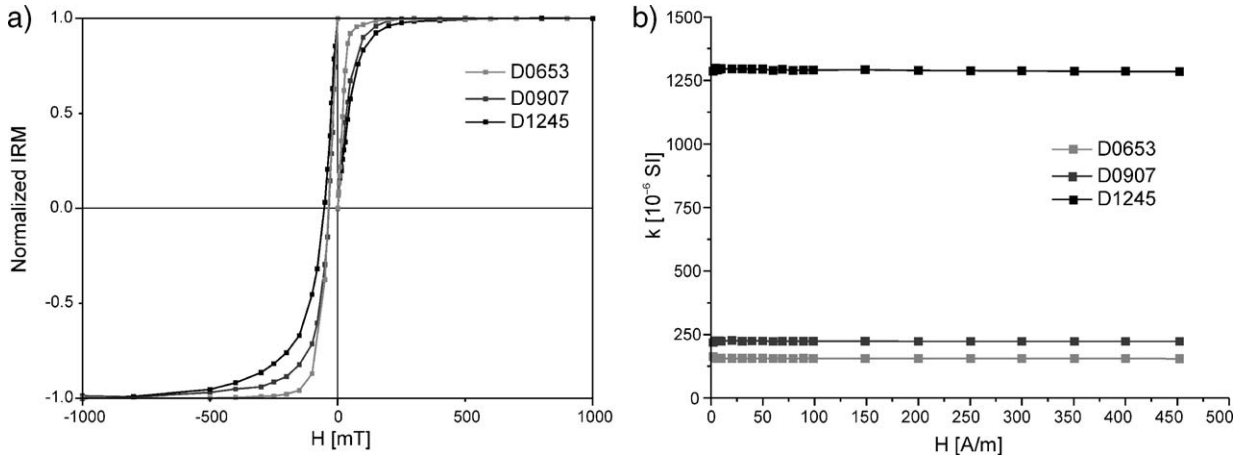

Fig. 5. (a) An isothermal remanent magnetization (IRM) for the three test samples acquired progressively in fields up to 1 T and backfield IRM acquired in the field up to 1 T in opposite direction. (b) The bulk magnetic susceptibility measured as a function of applied AC field with the intensity gradually increased from 2 to 450 A/m.

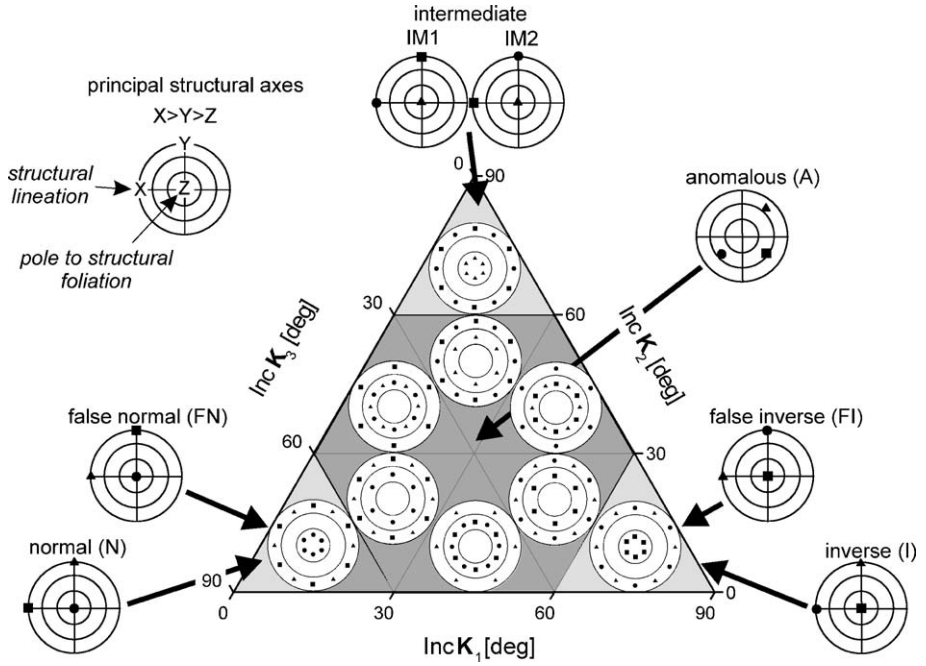

Fig. 6. A model ternary diagram interrelating inclinations of the principal anisotropy directions ($\mathbf{K}_1$, $\mathbf{K}_2$, $\mathbf{K}_3$) in bedding coordinate system. The 30° and 60° threshold angles subdivide the diagram into nine fields. Schematic stereoplots depicting the orientation of principal directions are drawn for each field. Different types of magnetic fabrics as defined by Rochette et al. (1992, 1999), and Ferré (2002) are presented outside of diagram. Square, triangle, and circle symbols represent maximum, intermediate, and minimum anisotropy directions, respectively.

lower right vertices, respectively, whereas the intermediate fabrics plot close to the upper vertex. Samples plotted in the hexagonal area in the center of the diagram can be regarded as anomalous. The advantage of the presented diagram is that the different transitions between the end-member magnetic fabrics (normal, inverse, and intermediate) can be quantitatively described.

5.2. Low-field magnetic anisotropy

Magnetic fabric (AMS) of the studied shales is more or less coaxial with the bedding. For the majority of samples, the magnetic lineation ($\mathbf{K}_1$) is subparallel to the bedding plane or, in some cases, perpendicular to it. No distinct preferred orientation of magnetic lineation within the bedding plane is observed (Fig. 7a). The absence of the cluster-like distribution of magnetic lineations suggests that magnetic lineation reflects neither paleocurrent direction nor the incipient stage of deformation when magnetic lineations tend to cluster in the direction perpendicular to the bedding-parallel shortening (Kligfield et al., 1983) or parallel to stretching direction in extensional basins (Sagnotti et al., 1994; Mattei et al., 1997; Cifelli et al., 2005). The direction of $\mathbf{K}_3$ (pole to magnetic foliation) is usually sub-normal to the bedding plane or, in some cases, subparallel to it or randomly oriented (Fig. 7b).

Although the low-field magnetic susceptibility varies widely, ranging from 84×10^{-6} to 2030×10^{-6} SI, the susceptibility values are lower than 250×10^{-6} SI for the majority of samples (Fig. 7c). The low susceptibility values may imply that the paramagnetic minerals dominate the magnetic susceptibility.

The shape of the AMS ellipsoid was plotted as a function of the anisotropy degree (Fig. 7d). Three distinct groups of samples can be distinguished: i) samples possessing prolate anisotropy ($T<-0.6$, henceforth denoted as the prolate-fabric samples) and a wide range of anisotropy degrees ($1<P<1.16$), ii) samples possessing triaxial shape ($-0.5<T<0.6$, the triaxial-fabric samples) with less variable anisotropy degree (generally $1.03<P<1.09$), and iii) samples characterized by the oblate shape ($T>0.6$, the oblate-fabric samples) and by wide range of anisotropy degrees ($1<P<1.16$). The above-described division is also reflected by the magnetic susceptibility (Fig. 7d); the highest susceptibility (usually, $k>300\times10^{-6}$ SI) is observed in the group of the prolate-fabric samples, whereas the oblate-fabric samples possess significantly lower susceptibility (usually, $k<300\times10^{-6}$ SI). The lowest magnetic susceptibility is possessed by the

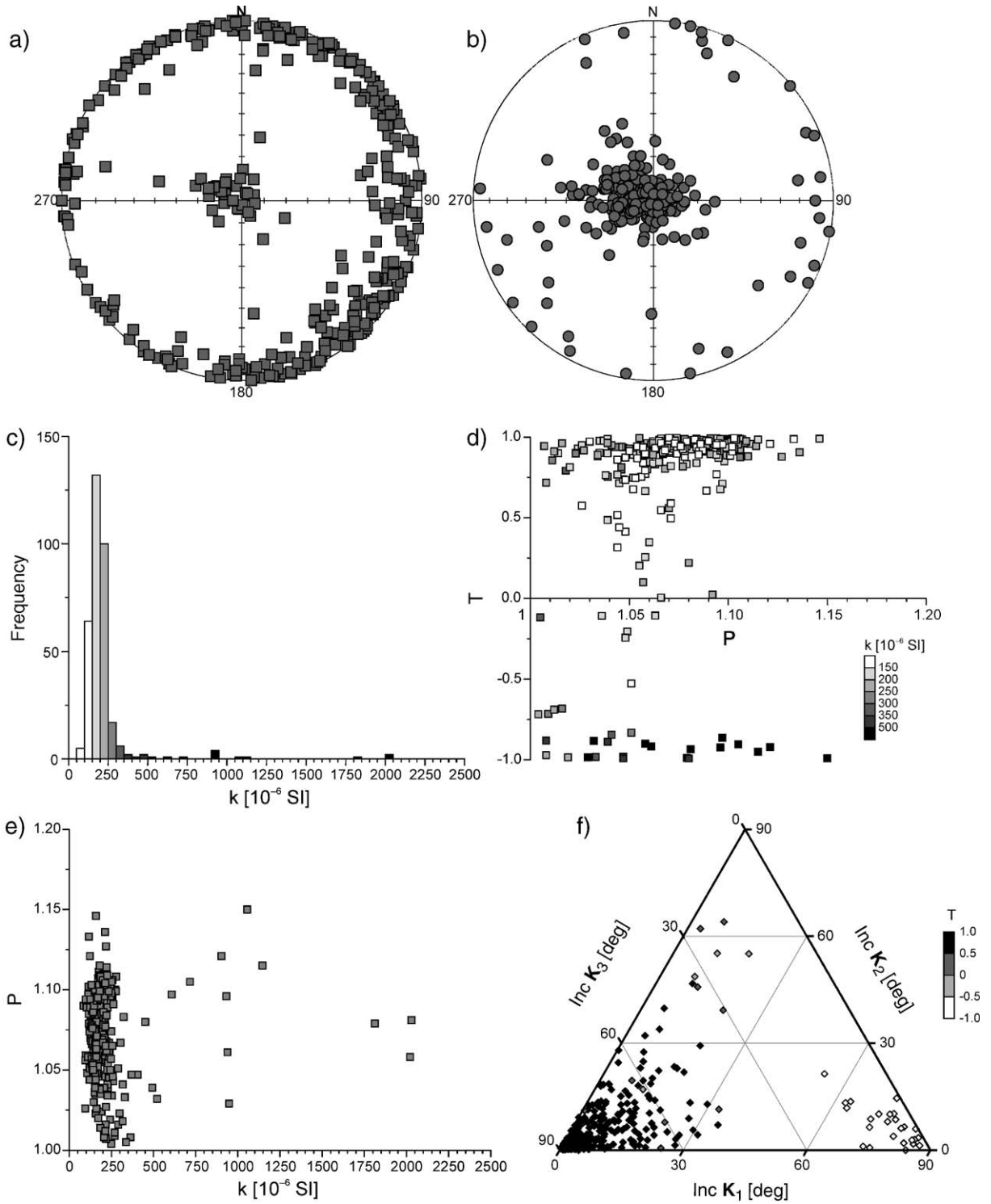

Fig. 7. The anisotropy of low-field magnetic susceptibility (AMS) for the entire set of samples. The maximum (a) and minimum (b) susceptibility directions are plotted in the equal-area projection on the lower-hemisphere in bedding coordinate system (tilt correction). Frequency distribution of the susceptibility values (c), relationship between anisotropy degree and shape of anisotropy ellipsoid (P–T plot) and magnetic susceptibility as grayscales (d), anisotropy degree (P) as a function of magnetic susceptibility (e), and ternary diagram relating the inclination angles of maximum, intermediate, and minimum susceptibility directions in the bedding coordinate system with the shape parameter (T) of anisotropy ellipsoids as grayscales (f).

triaxial-fabric samples (usually, $k<200\times10^{-6}$ SI). No apparent correlation between the magnetic susceptibility and the degree of anisotropy is observed (Fig. 7e).

As already evident from Fig. 7a, b, d, at least two different types of magnetic fabric (normal and inverse) can be distinguished. The orientation of the principal susceptibility axes is in the close relationship to the shape of the susceptibility ellipsoids (Fig. 7f). The majority of normal-fabric or inverse-fabric samples possess oblate or prolate shape, respectively. Despite the presence of triaxial-fabric samples (Fig. 7d) almost no pure intermediate fabric (cf., Rochette et al., 1999) is present but there are some samples that display a gradual transition from normal to intermediate fabric. The transitional samples possess both oblate and triaxial susceptibility ellipsoids (Fig. 7d). The group of inverse fabric samples is more distinctly delimited (Fig. 7f).

5.3. High-field anisotropy and anisotropy of magnetic remanence

For the representative oblate-, triaxial-, and prolate-fabric samples, the HFA (6 samples) and AARM (18 samples) were measured in order to separate the paramagnetic and ferromagnetic component of magnetic anisotropy. All the examined samples show a very similar linear dependence of the torque force as a function of the square of the applied field (Fig. 8). The 2Θ term of the Fast Fourier Transformation for all three perpendicular planes intersects at the origin, therefore the resolution of the HFA into paramagnetic (henceforth

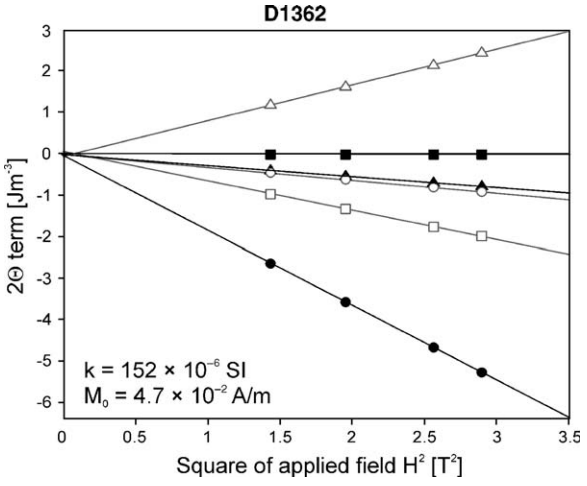

Fig. 8. Amplitude of the 2Θ-term as a function of the square of the applied field (B^2) for the three perpendicular measurement planes (squares, triangles, and circles) for sample D1362 where black symbols represent the coefficients of the cosine term and open symbols those of the sine term.

denoted as HFP) and ferrimagnetic components shows that the ferrimagnetic fraction, if present, appears to be insignificant (Martín-Hernández and Hirt, 2001).

All the samples selected for the AARM measurement can be magnetized and demagnetized with at least two orders of magnitude difference in magnetization between the magnetized and demagnetized states. Such a difference is a prerequisite for the successful application of the AARM method. The calculated remanent tensors represent the anisotropy carried by the ferromagnetic grains characterized by a particular coercivity, size and shape (Jackson et al., 1988).

The obtained data indicate that magnetic subfabrics carried by the paramagnetic and ferromagnetic grains are usually coaxial with the AMS. In some cases, only one pair of the respective principal directions (maximum or minimum) is subparallel. For the description of the orientation AARM or HFP subfabrics, the terms normal, inverse, intermediate, and anomalous magnetic fabric will be used in the relationship to the AMS in the following text. Hereafter, the normal AARM or HFP fabric is referred to the case when all three respective principal directions of the AARM or HFP are parallel to the AMS principal directions. Similarly, the inverse AARM or HFP fabric is characterized by the interchange of the maximum and minimum principal directions of the AARM or HFP and the AMS.

In the group of the prolate-fabric samples, the HFP fabric is normal with respect to the AMS, i.e. all three principal directions of the HFP and AMS are subparallel (Fig. 9, samples D1010, D1069). Both the AMS and HFP fabrics are inverse with respect to the bedding plane. The AARM is inverse or false inverse to the AMS, and normal to the bedding plane (Fig. 9).

In the group of the triaxial-fabric samples, the HFP fabric is false normal (Fig. 9, D0593, D1058), or anomalous with respect to the AMS (D1362). With respect to the bedding plane, the HFP fabric is normal (D1058, D1362) or inverse (D0593). The AARM fabric is usually normal (D0923, D0872, D1274, D1309, D1215) or false normal (D1176) to the AMS.

In the group of the oblate-fabric samples, the HFP fabric is normal with respect to the AMS and to the bedding plane (Fig. 9, D1033). The AARM fabric is normal (D1276, D1253, D1315) or false normal (D1279, D1118, D1086) to the AMS. In all cases, the magnetic foliation is subparallel to the bedding plane.

The shapes of AMS, AARM, and HFP ellipsoids are correlated quantitatively (Fig. 10). The samples with prolate AMS fabric show triaxial to oblate shapes compared to their AARM ellipsoids (Fig. 10a). For the triaxial AMS fabric samples, the shape of the AARM

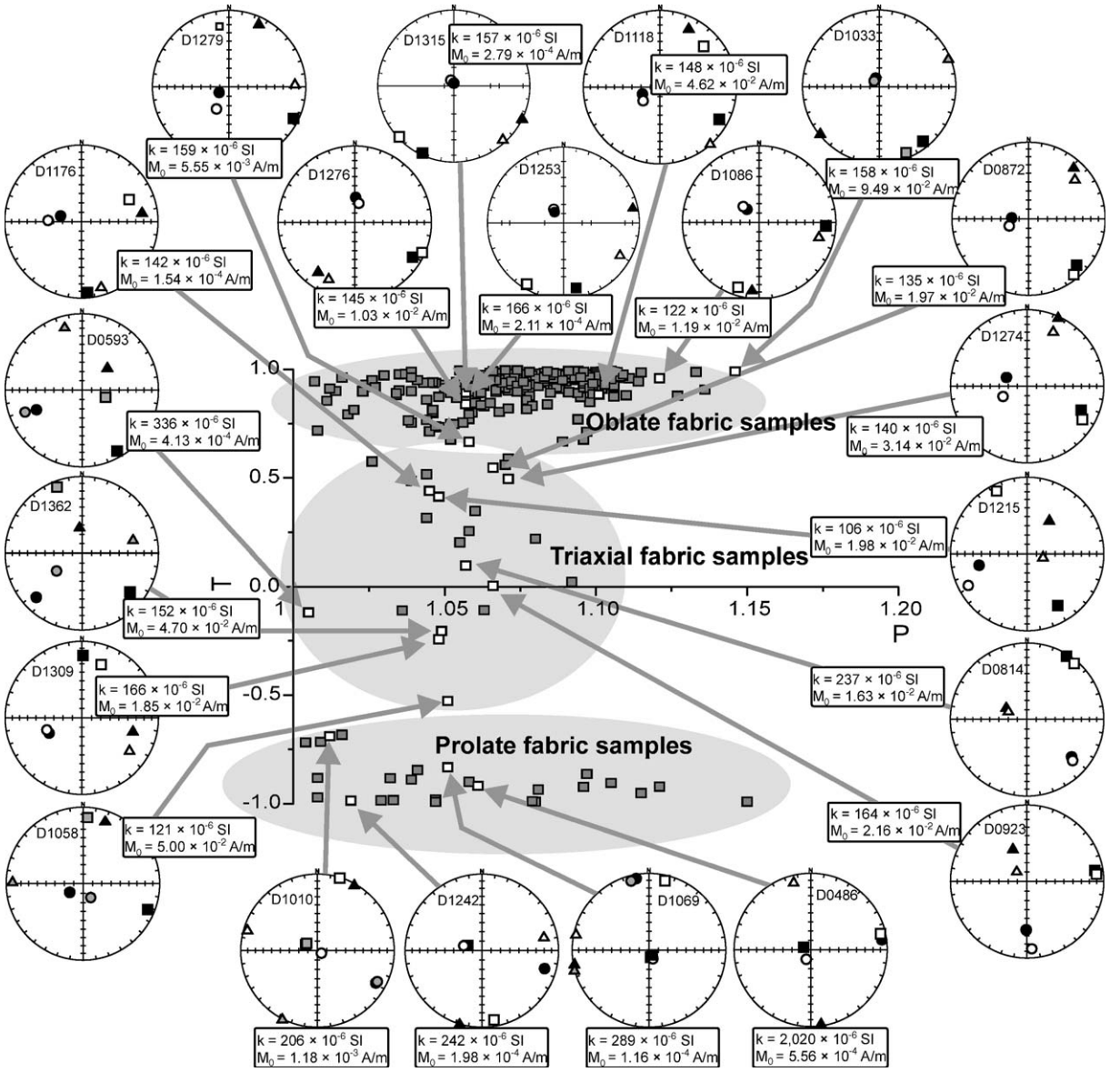

Fig. 9. The anisotropy degree vs. ellipsoid shape (P–T) plot of the AMS with equal-area, lower-hemisphere projections of the principal directions of the AMS (black symbols), high-field paramagnetic anisotropy (gray symbols), and anisotropy of anhysteretic magnetic remanence (open symbols) tensors in bedding coordinate system. Square, triangle, and circle symbols represent maximum, intermediate, and minimum anisotropy directions, respectively. Low-field magnetic susceptibility (k), and natural remanent magnetization (M_0) value are added for each sample.

ellipsoid varies significantly in the oblate to triaxial field, where a slight negative correlation can be seen. The oblate AMS fabric samples possess oblate shapes of the AARM ellipsoids.

Considering the HFP ellipsoids, the prolate AMS fabric samples have distinctly prolate shapes of the HFP ellipsoids (Fig. 10b). The behavior of the triaxial AMS fabric samples is more complex. Sample D0593 possesses triaxial shape of the HFP ellipsoid falling on the one-to-one correlation line whereas samples D1058, and D1362 possess oblate shapes of the HFP ellipsoids. The oblate AMS fabric sample D1033 has a distinctly oblate HFP ellipsoid.

5.4. Natural remanent magnetization and AF demagnetization

In order to isolate the characteristic remanent magnetization component (ChRM), stepwise AF demagnetization with measurement of the NRM

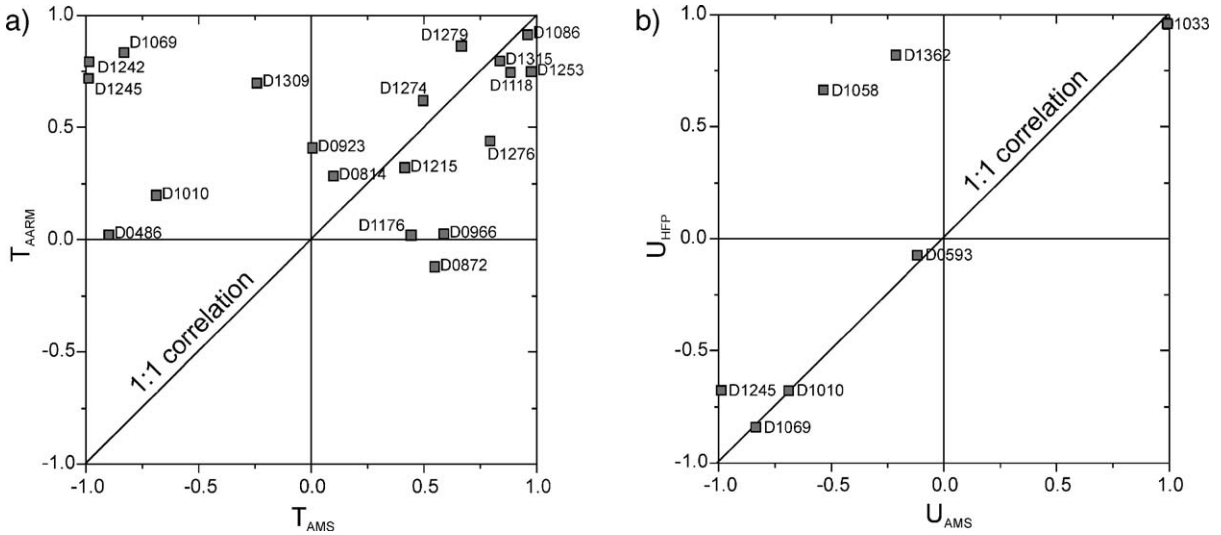

Fig. 10. Correlation between the shape of the AMS (T_{AMS}) and AARM (T_{AARM}) ellipsoids (a), and the shape of the AMS (U_{AMS}) and HFP (U_{HFP}) ellipsoids. The AMS represents the whole rock anisotropy, whereas the AARM or HFP represent the ferromagnetic or paramagnetic anisotropy components, respectively.

after each demagnetization step was carried out. The NRM values before any AF treatment, M_0, vary significantly from 6.47×10^{-5} to 9.42×10^{-2} A/m (Fig. 11a). A distinct group of samples with relatively high M_0 ($M_0>5\times10^{-3}$ A/m) is present, henceforth denoted as the high-NRM samples. After the AF treatment, all the samples successfully demagnetized usually to less than 1% of the original $_0$ value. As an indirect measure of magnetic coercivity, the medium destructive field (MDF)–the AF field at which half the M_0 is lost – was calculated from demagnetization curves for each sample. It is clearly seen that the majority of samples demagnetize to half of the M_0 in the field lower than 35 mT (Fig. 11b). The high-NRM samples demagnetize in the narrow coercivity window between 20 and 30 mT (Fig. 11b). The high MDF (MDF>35 mT) is bound to the reverse-polarity samples possessing two antiparallel components of NRM. Due to the normal to reverse polarity transition, the samples are demagnetized to half of the M_0 in relatively high AF fields (Fig. 11b). There is no simple correlation between the M_0 and magnetic susceptibility values (Fig. 11c). The group of high-susceptibility samples possess relatively low M_0 values whereas the high-NRM samples always have magnetic susceptibility lower than 250×10^{-6} SI. In the correlation between the M_0 and the quantitative AMS parameters, the high-NRM samples possess either oblate or triaxial AMS (Fig. 11d). Despite the even distribution of the high-NRM samples, it is evident that all the triaxial-fabric samples are characterized by high M_0 values. On the other hand, the prolate-fabric samples possess relatively low M_0 values. No statistical dependence was found between M_0 and the ratio between SIRM and magnetic susceptibility (Fig. 11e). Plotting the *S*-ratio for a backfield of 300 mT against M_0 shows that the high-NRM samples have a slightly higher *S*-ratio with an average value of 0.98×0.02. However, it is not greatly different from the remaining samples which have an average *S*-ratio of 0.96×0.02 (Fig. 11f).

6. Discussion and paleomagnetic implications

As evident from the anisotropy and NRM measurements, several different groups of sample behavior can be distinguished. The first group is represented by the samples with prolate inverse fabric (Fig. 7d, f) possessing the highest magnetic susceptibility (Fig. 7d), and relatively low M_0 values (Fig. 11d). In the studied sections these high-susceptibility inverse-fabric samples are usually bound to the concretions and cemented layers. The HFP fabric, which reflects the paramagnetic component of the magnetic anisotropy, is parallel to the AMS and inverse to the bedding plane. On the other hand, the AARM fabric, which is only due to the ferromagnetic component of the magnetic anisotropy, is always normal to the bedding plane (Fig. 9). In the cemented layers, the iron-bearing carbonate siderite was sometimes macroscopically observed. Siderite is common in hydrothermal mineralizations but is also encountered in sediments as a result of diagenesis under

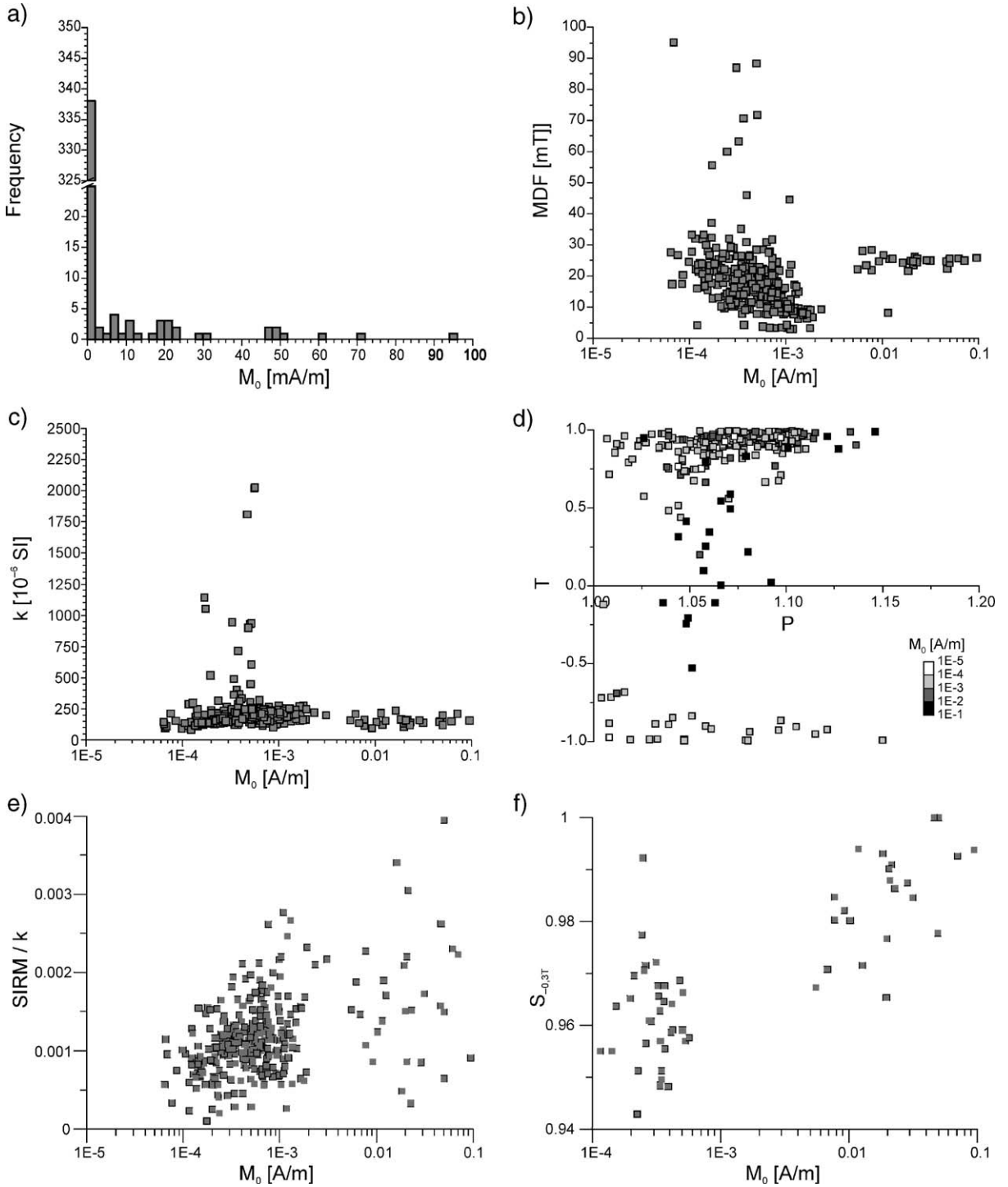

Fig. 11. The natural magnetic remanence (NRM) for the entire set of samples. Frequency distribution of the M_0 (a), relationship between M_0 and medium destructive field (MDF) (b), relationship between M_0 and magnetic susceptibility (c), and the AMS P–T plot with M_0 values of respective samples plotted as grayscales (d), relationship between M_0 and SIRM/k ratio (e), and the relationship between M_0 and S-ratio calculated from the SIRM and IRM acquired in the field of 0.3 T in opposite direction, for selected samples only (f).

anoxic conditions (Ellwood et al., 1988). Siderite is a paramagnetic mineral characterized by an inverse relationship between the crystallographic axes and the AMS principal axes (Jacobs, 1963). This suggests that the AMS in the inverse-fabric samples is controlled by the presence of siderite crystals distributed with the *c*-crystallographic axis normal to the bedding plane. The bedding parallel AARM fabric reflects the minor presence of a ferromagnetic fraction distributed within the bedding plane. The presence of siderite in the prolate-fabric samples was further verified by XRD analysis (Fig. 3, D1245, Table 2). During the laboratory heating, the magnetic susceptibility of the siderite-bearing samples decreases up to 300 °C following paramagnetic behavior. Susceptibility resolution into paramagnetic and ferromagnetic components showed that magnetic susceptibility is almost entirely carried by paramagnetic component (Fig. 2, D1245). The rapid susceptibility increase above the temperature of 300 °C can be attributed to the laboratory induced mineral changes; siderite is transformed to maghemite, and later, to magnetite or hematite (Ellwood et al., 1986; Hirt and Gehring, 1991; Pan et al., 2000) as evidenced by the susceptibility decrease above approximately 550 °C (Fig. 2). If the high-susceptibility and the inverse-HFP-fabric criteria are applied, it seems probable that the magnetic anisotropy of the triaxial-fabric sample D0593 is also siderite controlled (Figs. 9 and 10b). On the other hand, the HFP fabric of the prolate to triaxial samples D1058 and D1362 is more or less bedding controlled (Figs. 9 and 10b). Moreover, these samples possess relatively low magnetic susceptibility ($k<152\times10^{-6}$, Fig. 7d), and relatively high M_0 values ($M_0>4.7\times10^{-2}$, Fig. 11d).

After AF demagnetization, two stable components of the NRM can be isolated for the majority of the siderite-bearing samples (Fig. 12a): a low-field component (approximately 5–15 mT), and a high-field component (15–80 mT), regarded as ChRM component. The mean direction of the ChRM component is $D=46.5°$, $I=85.6°$, $k=21.6$, $\alpha_{95}=6.3°$ (Fig. 12b). This direction is in agreeement with the magnetic field for the J/K (Savostin et al., 1993). For all the siderite-bearing samples, only normal magnetic polarity is present (Fig. 12b). Although the magnetization of the siderite-bearing samples may have been acquired during the diagenesis of the sediment, the absence of the reverse polarity magnetization is suggestive of remagnetization. For this reason, the siderite-bearing samples were excluded from further magnetostratigraphic study.

The group of the triaxial-fabric samples possesses a relatively low magnetic susceptibility (Fig. 7d) but the highest M_0 values (Fig. 11d). These high M_0 values are not exclusively found in the triaxial-fabric samples but can be observed for some oblate-fabric samples as well. Since the high M_0 value is the characteristic feature of the triaxial-fabric samples, it seems probable that the high M_0 value is not the response to subsequent magnetization, possibly artificially imparted, but is a material feature of this particular group of samples. The high-NRM samples possessing both intermediate and normal fabric will be considered as one distinct group in further discussion. The HFP foliation is close to the bedding plane (Fig. 9, D1058, D1362, D1033) and the fabric is distinctly oblate (Fig. 10b). The ferromagnetic fabric, reflected by AARM, is coaxial with the AMS (Fig. 9) and triaxial in shape (Fig. 10a). As shown by the linear dependence of the torque moment to the square of the applied field, the paramagnetic minerals are the dominant components of the magnetic anisotropy (Fig. 8). It appears that the paramagnetic mineral, which has normal magnetic fabrics, most probably iron-bearing chlorite or mica (Fig. 3 and Table 2), is the main carrier of magnetic anisotropy. The dominance of paramagnetic mineral(s) on bulk susceptibility can be evidenced by the magnetic susceptibility versus temperature curve during laboratory heating up to 240 °C. The curve follows a paramagnetic behavior and susceptibility resolution into paramagnetic and ferromagnetic component shows that the paramagnetic contribution to the room temperature magnetic susceptibility is approximately 80% (Fig. 2, D0653). The two-step increase of magnetic susceptibility in the temperature interval of 240–400 °C may be attributed (1) to decomposition of an iron hydroxide or phase transition in pyrrhotite (Dekkers, 1989; Zapletal, 1993); (2) the decomposition of berthierine, an iron-rich clay mineral found in ferruginous rocks (Hirt and Gehring, 1991); or (3) to the gradual changes in iron sulfide mineralogy (Krs et al., 1992). Further susceptibility increase can be attributed to the thermal decomposition of pyrite and its conversion to magnetite. The abundant presence of pyrite in the high-NRM samples was evidenced by XRD (Fig. 3 and Table 2). The pyrite decomposition at about 400–440 °C has been verified by XRD thermal scans (not presented). The presence of newly created magnetite is verified by a sharp susceptibility decrease at approximately 550 °C.

In order to explain the ferromagnetic mineralogy in the high-NRM triaxial-fabric samples, several hypotheses were proposed. An iron sulfide may explain the high M_0 intensities and triaxial-fabrics, but there is no

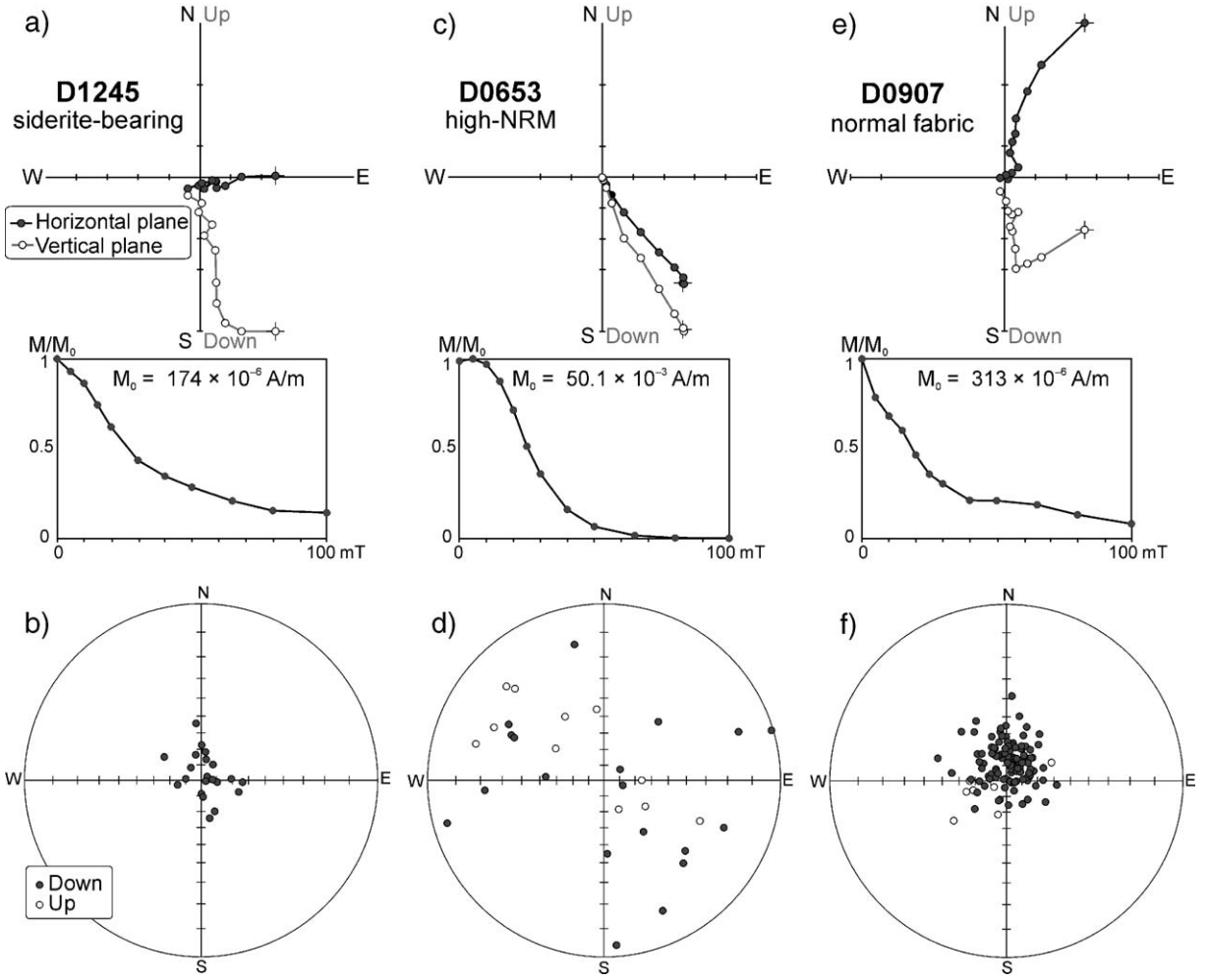

Fig. 12. Zijderveld diagrams of the AF demagnetizations for representative test samples (a, c, e), and directions of the characteristic remanence components for the entire group of samples (b, d, f, gray and open symbols represent normal or reverse polarity, respectively), all in the tilt correction coordinate system.

evidence that the ferromagnetic mineralogy of these samples different from the other samples. Susceptibility did not show any field dependence as would be expected for pyrrhotite (Fig. 5b), and relatively low SIRM/*k* ratios (Fig. 11e), and high *S*-ratio which is indicative of presence of the low coercivity mineral, i.e. magnetite (Fig. 11f) precludes greigite as a carrier of the NRM. Moreover, the MDF of the high-NRM samples in the range of 20–30 mT is generally too low with respect to the values reported for greigite (Dekkers and Schoonen, 1996) or pyrrhotite (Dekkers, 1988).

Another possible explanation of the magnetic mineralogy of the high-NRM samples may be the presence of antiferromagnetic goethite which decomposition is suggested by thermal changes of bulk magnetic susceptibility (Fig. 2). The interference of the inverse magnetic fabric carried by goethite with the normal magnetic fabric due to the paramagnetic matrix was responsible for anomalous magnetic fabric in several horizons of Pleistocene marine sequence in central Italy (Lehman et al., 1996). The reported anomalous magnetic fabric was almost isotropic with a very low magnitude of anisotropy. This observation is in correspondence with the triaxial fabric possessing a relatively low degree of anisotropy (Fig. 9). Despite these indirect clues the presence of goethite has to be rejected according to IRM acquisition curves where all the test samples reached the SIRM at about 0.5 T (Fig. 5a). The H_{cr} values are also very low compared to the data published for goethite (Peters and Dekkers, 2003).

Intermediate magnetic fabric for the group of the triaxial-fabric samples could be possibly explained by the substrate-controlled growth of siderite crystal along the bedding plane as described by Hounslow (2001). In

such a situation the *c*-axes of siderite are oriented obliquely to the bedding plane resulting in the oblique magnetic fabric as observed in the siderite-bearing pelitic rock in SW England (de Wall and Warr, 2004). Although siderite is abundant in the siderite concretion and siderite-cemented layer its presence was not found in the high-NRM samples (Fig. 3 and Table 2). The magnetic susceptibility of this group of samples is relatively low as opposed to the siderite-bearing inverse-fabric samples where the highest susceptibility values were measured (Fig. 7d). Moreover, the group of inverse-fabric siderite-bearing samples is rather distinctly delimited (Fig. 7f). It seems probable that the substrate-controlled growth of siderite crystals is not the mechanism responsible for the intermediate magnetic fabric in the high-NRM samples.

Despite the above-outlined hypothesis, all the rock magnetic measurements on the test samples, as well as SIRM, and the *S*-ratio values show no significant difference between the group of normal-fabric and high-NRM samples. The normalized IRM acquisition curves, low H_{cr} values (Fig. 5a) and high *S*-ratio (Fig. 11f), are indicative for Ti-poor magnetite as the main carrier of NRM in both normal-fabric and high-NRM samples.

After the AF demagnetization, only one stable component of the NRM can be isolated (5–80 mT) for the majority of the high-NRM samples (Fig. 12c). Although both magnetic polarities are present, the directions are highly scattered (Fig. 12d). Consequently, the mean direction for samples with normal polarity is $D=152.0°$, $I=78.2°$, $k=1.8$, $\alpha_{95}=37.5°$ and reverse polarity, $D=320.4°$, $I=-61.8°$, $k=2.9$, $\alpha_{95}=33.2$. Due to the high directional scatter, the ChRM isolated from the high-NRM samples cannot be used for intended magnetostratigraphic research. The magnetic mineralogy of these samples is not different from the other samples, therefore it is not possible to speculate on why these samples are not a good recorder of the ancient field.

The group of the oblate-fabric samples comprises both relatively low and high-NRM samples (Fig. 11d). The AMS, HFP, and AARM fabrics are more or less controlled by the bedding plane (Fig. 9, D1279, D1276, D1315, D1253, D1118, D1086), whereby the maximum and intermediate directions of AMS and AARM may be mutually interchanged. All types of magnetic fabric (AMS, HFP, AARM) are oblate in shape (Fig. 10a, b). It appears that the AMS is controlled by the preferred orientation of the paramagnetic phyllosilicates which dominate the XRD scans (Fig. 3).

After the AF demagnetization, two stable components of the NRM can be usually isolated (Fig. 12e) where the high-field component is regarded as the ChRM. Both magnetic polarities are present for the ChRM. The mean directions for the normal and reverse polarities are $D=7.1°$, $I=77.9°$, $k=21.7$, $\alpha_{95}=2.9°$ and $D=276.9°$, $I=-68.3°$, $k=6.8$, $\alpha_{95}=11.8°$, respectively. The high inclination of normal and reverse mean directions is in agreement with the magnetic field direction for the J/K (Fig. 12f).

7. Conclusions

In this study of the Mesozoic black shales on the northern margin of the Siberian Craton, we have shown that the low-field magnetic susceptibility is predominately carried by the paramagnetic minerals, i.e. iron carbonate siderite, iron-bearing chlorites, and micas. Despite this fact, the influence of ferromagnetic fraction on the magnetic properties of some samples cannot be neglected. According to the magnetic anisotropy behavior and NRM, three main groups of samples can be distinguished: i) siderite-bearing samples that are characterized by an inverse prolate magnetic fabrics, usually accompanied by relatively high magnetic susceptibility values ($k>300\times10^{-6}$ SI), ii) a triaxial- to oblate-fabric samples possessing high M_0 intensities that are one to two orders of magnitude higher than average M_0, and iii) oblate-fabric samples with a relatively low M_0 values. There is no apparent correlation between the high susceptibility and high M_0 values; on the contrary, the high M_0 excludes the high susceptibility, and vice versa.

The low-field magnetic anisotropy in the siderite-bearing rocks (i) is controlled by the preferred orientation of siderite known for its inverse magnetic anisotropy. The ferromagnetic anisotropy, determined by the AARM, is oblate in shape and controlled by bedding compaction. Two stable components of the NRM can be isolated for the majority of the siderite-bearing samples. The high-field component, regarded as the ChRM, is characterized by absence of reverse-polarity samples, suggesting that this component is a secondary magnetization, most likely of chemical origin. For this reason, the siderite-bearing samples will be excluded from the magnetostratigraphic investigation.

The magnetic mineralogy of the high-NRM, triaxial- to oblate-fabric samples (ii) is more complex. The AMS is mainly controlled by the paramagnetic, and to the lesser extent by ferromagnetic fraction. Ferromagnetic minerals are probably of detrital origin. Only one stable component of the NRM can be isolated for the majority of the high-NRM samples. Although both magnetic

polarities of the ChRM are present, the directions are highly scattered. The anomalous AMS results and the scattered ChRM directions also suggest that the magnetic mineralogy has undergone some change in the past. These samples will also be excluded from the magnetostratigraphic study.

The magnetic anisotropy in the group of the oblate-fabric samples (iii) is predominantly controlled by the preferred orientation of iron-bearing chlorites or micas, and to a minor extent, by the ferromagnetic fraction. Two stable components of magnetization can be usually isolated. Both magnetic polarities are present for the high coercivity ChRM. The oblate, bedding-controlled fabric, and the low M_0 suggests that these samples may be good recorders of the ancient field and therefore useful for magnetostratigraphic study across J/K boundary. This group represents approximately 85% of the entire sample set, and covers evenly the entire length of the studied section.

Acknowledgements

The authors gratefully acknowledge the colleagues with whom they made a field party in the tough arctic conditions in August 2003: V. Zakharov, M. Rogov, M. Košt'ák, and M. Mazuch. Laboratory measurements and some data processing were carried out by N. Nowaczyk, P. Vorm, P. Bezdička, V. Goliáš, Z. Korbelová, A. Langrová, and J. Petráček. The comments and suggestions from L. Sagnotti and anonymous reviewer and discussion with E. Petrovský considerably improved the manuscript. The attendance at the AGU 2004 Fall Meeting was supported by Hlávka Foundation, Prague. The research was supported by the Czech Science Foundation Research Grant #205/02/1576.

References

Bergmüller, F., Bärlocher, C., Geyer, B., Grieder, M., Heller, F., Zweifel, F., 1994. A torque magnetometer for measurements of the high-field anisotropy of rocks and crystals. Meas. Sci. Technol. 5, 1466–1470.

Bloemendal, J., King, J.W., Hall, F.R., Doh, S.-J., 1992. Rock magnetism of Late Neogene and Pleistocene deep-sea sediments: relationship to sediment source, diagenetic processes and sediment lithology. J. Geophys. Res. 97, 4361–4375.

Borradaile, G.J., Gauthier, D., 2001. AMS-detection of inverse fabrics without AARM, in ophiolite dikes. Geophys. Res. Lett. 28, 3517–3520.

Cifelli, F., Mattei, M., Chadima, M., Hirt, A.M., Hansen, A., 2005. The origin of tectonic lineation in extensional basins: combined neutron and magnetic analyses on "undeformed" clays. Earth Planet. Sci. Lett. 235, 62–78.

Dekkers, M.J., 1988. Magnetic properties of natural pyrrhotite: I. Behaviour of initial susceptibility and saturation–magnetization-related rock-magnetic parameters in a grain-size dependent framework. Phys. Earth Planet. Inter. 52, 376–393.

Dekkers, M.J., 1989. Magnetic properties of natural pyrrhotite: II. High- and low-temperature behaviour of J_{rs} and TRM as function of grain size. Phys. Earth Planet. Inter. 57, 266–283.

Dekkers, M.J., Schoonen, M.A.A., 1996. Magnetic properties of hydrothermally synthesized greigite (Fe_3S_4): I. Rock magnetic parameters at room temperature. Geophys. J. Int. 126, 360–368.

de Wall, H., Warr, L.N., 2004. Oblique magnetic fabric in siderite-bearing pelitic rocks of the Upper Carboniferous Culm Basin, SW-England: an indicator for palaeo-fluid migration? In: Martín-Hernández, F., Lüneburg, C.M., Aubourg, C., Jackson, M. (Eds.), Magnetic Fabric: Methods and Applications. Geol. Soc. London, Special Publications, vol. 238, pp. 493–507.

Drachev, S.S., Savostin, L.A., Groshev, V.G., Bruni, I.E., 1998. Structure and geology of the continental shelf of the Laptev Sea, Eastern Russian Arctic. Tectonophysics 298, 357–393.

Ellwood, B.B., Balsam, W., Burkart, B., Long, G.J., Buhl, M.L., 1986. Anomalous magnetic properties in rocks containing the mineral siderite: Palaeomagnetic implications. J. Geophys. Res. 91, 12779–12790.

Ellwood, B.B., Chrzanowski, T.H., Hrouda, F., Long, G.J., Buhl, M. L., 1988. Siderite formation in anoxic deep-sea sediments: a synergic bacterially controlled process with important implications in paleomagnetism. Geology 16, 980–982.

Ellwood, B.B., Burkart, B., Rajeshwar, K., Darwin, R.L., Neeley, R. A., McCall, A.B., Long, G.J., Buhl, M.L., Hickcox, C.W., 1989. Are the iron carbonate minerals, ankerite, and ferroan dolomite, like siderite, important in paleomagnetism? J. Geophys. Res. 94 (B6), 7321–7331.

Ferré, E.C., 2002. Theoretical models of intermediate and inverse AMS fabrics. Geophys. Res. Lett. 29 (31), 1–4.

Ferré, E.C., Améglio, L., 2000. Preserved magnetic fabric vs. annealed microstructures in the syntectonic recrystallised George granites, South Africa. J. Struct. Geol. 22, 1199–1219.

Fisher, R.A., 1953. Dispersion on a sphere. Proc. R. Soc. Lond., A 217, 295–305.

Hamilton, N., Rees, A.I., 1970. Magnetic fabric of sediments from the shelf at La Jolla (California). Mar. Geol. 9, M6–M11.

Hirt, A., Gehring, A., 1991. Thermal alteration of the magnetic mineralogy in ferruginous rocks. J. Geophys. Res. 96, 9947–9954.

Hounslow, M.W., 2001. The crystallographic fabric and texture of siderite in concretions: implications for siderite nucleation and growth processes. Sedimentology 48, 533–557.

Houša, V., Krs, M., Krsová, M., Man, O., Pruner, P., Venhodová, D., 1999. High-resolution magnetostratigraphy and micropalaeontology across the J/K boundary strata at Brodno near ilina, western Slovakia: summary of results. Cretac. Res. 20, 699–717.

Houša, V., Krs, M., Man, O., Pruner, P., Venhodová, D., Cecca, F., Nardi, G., Piscitello, M., 2004. Combined magnetostratigraphic, palaeomagnetic and calpionellid investigations across Jurassic/Cretaceous boundary strata in the Bosso Valley, Umbria, central Italy. Cretac. Res. 25, 771–785.

Hrouda, F., 1994. A technique for the measurement of thermal changes of magnetic susceptibility of weakly magnetic rocks by the CS-2 apparatus and KLY-2 Kappabridge. Geophys. J. Int. 118, 604–612.

Hrouda, F., Jelínek, V., Zapletal, K., 1997. Refined technique for susceptibility resolution into ferromagnetic and paramagnetic

components based on susceptibility temperature-variation measurement. Geophys. J. Int. 129, 715–719.
Ihmlé, P.F., Hirt, A., Lowrie, W., Dietrich, D., 1989. Inverse magnetic fabric in deformed limestones of the Morcles nappe, Switzerland. Geophys. Res. Lett. 16, 1383–1386.
Jackson, M., Gruber, W., Marvin, J., Banerjee, S.K., 1988. Partial anhysteretic remanence and its anisotropy: application and grain size-dependence. Geophys. Res. Lett. 15, 440–443.
Jacobs, I.S., 1963. Metamagnetism of siderite. J. Appl. Phys. 34, 1106–1107.
Jelínek, V., 1981. Characterization of the magnetic fabric of rocks. Tectonophysics 79, T63–T67.
Jelínek, V., 1993. Theory and measurement of the anisotropy of isothermal remanent magnetization of rocks. Trav. Geophys. 37, 124–134.
Kirschvink, J.L., 1980. The lest-squares line and plane and the analysis of palaeomagnetic data. Geophys. J. R. Astron. Soc. 62, 699–718.
Kligfield, R., Lowrie, W., Hirt, A.M., Siddans, A.W.B., 1983. Effect of progressive deformation on remanent magnetization of Permian redbeds from the Maritime Alps (France). Tectonophysics 97, 59–85.
Krs, M., Novák, F., Krsová, M., Pruner, P., Kouklikóvá, L., Jansa, J., 1992. Magnetic properties and metastability of greigite–smythite mineralization in brown-coal basins of the Krusne hory Piedmont, Bohemia. Phys. Earth Planet. Inter. 70, 273–287.
Lehman, B., Sagnotti, L., Winkler, A., Lo Cascio, C., 1996. Magnetic mineralogy changes in the Pleistocene marine sequence of Montalto di Castro (central Italy) and influence on the magnetic anisotropy. Geophys. J. Int. 127, 529–541.
Mattei, M., Sagnotti, L., Faccenna, C., Funiciello, R., 1997. Magnetic fabric of weakly deformed clay-rich sediments in the Italian peninsula: relationship with compressional and extensional tectonics. Tectonophysics 271, 107–122.
Martín-Hernández, F., Hirt, A.M., 2001. Separation of ferrimagnetic and paramagnetic anisotropies using a high-field torsion magnetometer. Tectonophysics 337, 209–221.
Nagata, T., 1961. Rock Magnetism, 2nd edition. Maruzen, Tokyo. 350 pp.
Pan, Y., Zhu, R., Banerjee, S.K., Gill, J., Williams, Q., 2000. Rock magnetic properties related to thermal treatment of siderite: behavior and interpretation. J. Geophys. Res. 105 (B1), 783–794.
Peters, C., Dekkers, M.J., 2003. Selected room temperature magnetic parameters as a function of mineralogy, concentration and grain size. Phys. Chem. Earth 28, 659–667.
Pokorný, J., Suza, P., Hrouda, F., 2004. Anisotropy of magnetic susceptibility of rocks measured in variable weak magnetic fields using the KLY-4S Kappabridge. In: Martín-Hernández, F., Lüneburg, C.M., Aubourg, C., Jackson, M. (Eds.), Magnetic Fabric: Methods and Applications. Geol. Soc. London, Special Publications, vol. 238, pp. 69–76.
Potter, D.K., Stephenson, A., 1988. Single-domain particles in rocks and magnetic fabric analysis. Geophys. Res. Lett. 15, 1097–1100.
Robion, P., Delamotte, D.F., Kissel, C., Aubourg, C., 1995. Tectonic versus mineralogical contribution to the magnetic fabric of epimetamorphic slaty rocks–a example from the Ardennes Massif (France–Belgium). J. Struct. Geol. 17, 1111–1124.
Rochette, P., 1988. Inverse magnetic fabric in carbonate-bearing rocks. Earth Planet. Sci. Lett. 90, 229–237.
Rochette, P., Jackson, M., Aubourg, C., 1992. Rock magnetism and the interpretation of anisotropy of magnetic susceptibility. Rev. Geophys. 30, 209–226.
Rochette, P., Scaillet, B., Guillot, S., Le Fort, P., Pecher, A., 1994. Magnetic properties of the High Himalayan leucogranites: structural implications. Earth Planet. Sci. Lett. 126, 217–234.
Rochette, P., Aubourg, C., Perrin, M., 1999. Is this magnetic fabric normal? A review and case studies in volcanic formations. Tectonophysics 307, 219–234.
Sagnotti, L., Faccena, C., Funicello, R., Mattei, M., 1994. Magnetic fabric and structural setting of Plio-Pleistocene clayey units in an extensional regime: the Tyrrhenian margin of Central Italy. J. Struct. Geol. 16, 1243–1257.
Savostin, L.A., Pavlov, V.E., Safonov, V.G., Bondarenko, G.E., 1993. Otlozheniya nizhney i sredney yuri na zapade Omolonskogo massiva (Severo-Vostok Rossii): usloviya obrazovaniya i paleomagnetism. Dokl. Acad. Sci. USSR 333, 481–486 (in Russian).
Winkler, A., Florindo, F., Sagnotti, L., Sarti, G., 1996. Inverse to normal magnetic fabric transition in an upper Miocene marly sequence from Tuscany, Italy. Geophys. Res. Lett. 23, 909–912.
Worm, H.-U., Clark, D., Dekkers, M.J., 1993. Magnetic susceptibility of pyrrhotite: grain size, field and frequency dependence. Geophys. J. Int. 114, 127–137.
Zakharov, V.A., Nal'nyaeva, T.I., Shul'gina, N.I., 1983. New results on biostratigraphy of Upper Jurassic and Lower Cretaceous strata in the Paksa Peninsula, Anabar Bay. In: Zakharov, V.A. (Ed.), Jurassic and Cretaceous paleobiogeography and biostratigraphy of Siberia. Nauka, Moscow, pp. 56–99 (in Russian).
Zakharov, V.A., Lapukhov, A.S., Shenfil, O.V., 1993. Iridium anomaly at the Jurassic–Cretaceous boundary in Northern Siberia. Russ. Geol. Geophys. 1, 83–90.
Zapletal, K., 1993. Effect of intergrowths of the ferrimagnetic and antiferromagnetic phases on the rock magnetic properties of natural pyrrhotites. Phys. Earth Planet. Inter. 76, 151–162.